Thermal and State-Selected Rate Coefficients for the O(^{3}P) + HCl Reaction and New Calculations of the Barrier Height and Width[†]

Sergei Skokov,[‡,§] Shengli Zou,[‡] Joel M. Bowman,*[,‡] Thomas C. Allison,*[,||]
Donald G. Truhlar,*[,⊥] Yongjing Lin,[#] B. Ramachandran,*[,#] Bruce C. Garrett,[×] and
Benjamin J. Lynch[⊥]

Department of Chemistry, Emory University, 1515 Pierce Drive, Atlanta, Georgia 30322,
Experimental Kinetics and Thermodynamics Group, National Institute of Standards and Technology,
100 Bureau Drive, Stop 8381, Gaithersburg, Maryland 20899-8381, Department of Chemistry and
Supercomputer Institute, University of Minnesota, Minneapolis, Minnesota 55455-0431, Chemistry,
P.O. Box 10348, Louisiana Tech University, Ruston, Louisiana 71272, and Environmental Molecular Sciences
Laboratory, Pacific Northwest National Laboratory, P.O. Box 999, Richland, Washington 99352

Received: October 16, 2000; In Final Form: December 12, 2000

This paper compares several approximate methods for calculating rate coefficients for the O(^{3}P) + HCl reaction to presumably more accurate quantum mechanical calculations that are based on applying the *J*-shifting approximation (QM/JS) to an accurate cumulative reaction probability for *J* = 0. All calculations for this work employ the recent S4 potential energy surface, which presents a number of challenges for the approximate methods. The O + HCl reaction also poses a significant challenge to computational dynamics because of the heavy−light−heavy mass combination and the broad noncollinear reaction path. The approximate methods for calculating the thermal rate coefficient that are examined in this article are quasiclassical trajectories (QCT), conventional transition state theory (TST), variational transition state theory employing the improved canonical variational theory (ICVT), ICVT with the microcanonical optimized multidimensional tunneling correction (ICVT/μOMT), and reduced dimensionality quantum mechanical calculations based on adiabatic bend and *J*-shifting (QM/AB-JS) approximations. It is seen that QCT, TST, and ICVT rate coefficients agree with each other within a factor of 2.7 at 250 K and 1.6 at l000 K, whereas inclusion of tunneling by the ICVT/μOMT, QM/AB-JS, or QM/JS methods increases the rate coefficients considerably. However, the ICVT/μOMT and QM/AB-JS methods yield significantly lower rate coefficients than the QM/JS calculations, especially at lower temperatures. We also report and discuss calculations for the state-selected reaction of O(^{3}P) with HCl in the first excited vibrational state. In addition to the dynamics calculations, we report new electronic structure calculations by the Multi-Coefficient Gaussian-3 (MCG3) method that indicate that one possible source of disagreement between the QM/JS rate coefficients and experiment is that the barrier on the S4 surface may be too narrow.

I. Introduction

The development of approximate methods for reaction dynamics is vital for the study of polyatomic systems because practical converged quantal calculations are restricted to few-body systems. However approximate methods should be validated against accurate quantum mechanical calculations as widely as possible in order to establish their reliability and range of applicability. The subject of this paper is the calculation of thermal and vibrational-state-selected rate coefficients for the O(^{3}P) + HCl → OH + Cl reaction using a variety of approximate dynamical methods. The rate coefficients obtained from these calculations are compared in the present paper to a set of results[1] based on accurate three-dimensional quantum mechanical calculations for total angular momentum *J* = 0 combined with the *J*-shifting approximation (QM/JS). All these dynamical calculations are based on the same potential energy surface (PES). This three-atom system poses many challenges for the dynamical methods employed due to the nature of the potential energy surface and the presence of two relatively massive atoms and one hydrogen.

The reaction is assumed to occur only on the ^{3}A″ electronic state of the three-atom system. The representation of this state used in the present study is the S4 PES of Ramachandran et al.[2] This surface is based on scaled[3] ab initio electronic structure calculations at the MR-CISD+Q/cc-pVTZ level.[2] Quasiclassical trajectory (QCT) calculations on the S4 surface have produced product rotational distributions, vibrational branching ratios,[2] and energy disposal patterns[4] in excellent agreement with the experiments of Zhang et al.[5] In this regard, the S4 PES appears to be more accurate than earlier potential surfaces based on scaled ab initio calculations.[6−8] However, more recent investigations by Skokov et al.[1] and Nobusada et al.[9] have indicated that

the reaction rate coefficients for the S4 surface are larger than experiment, indicating that the barrier may be too low or too thin or both.

The approximate methods reported in this paper can be classified into three broad categories: (I) those that do not account for tunneling; (II) those that include tunneling using semiclassical methods; (III) those that use quantum mechanics on an effective potential of reduced dimensionality. Included in the first category are QCT calculations,[10] conventional transition state theory (TST),[11] and variational transition state theory (VTST).[12-15] From among the range of algorithms that may be employed for the latter, we choose the improved canonical variational theory (ICVT)[13,14] as implemented in the program polyrate.[16] In category II, we consider ICVT calculations that incorporate semiclassically calculated tunneling contributions, obtained using the microcanonical optimized multidimensional tunneling (μOMT)[17] approximation for transmission coefficients. This method has been widely validated.[18,19] Finally, in category III is an approximate quantum mechanical method in which the adiabatic bend (QM/AB) approximation[20-22] is used to reduce the dimensionality and the *J*-shifting[23] approximation is used to obtain approximate results (QM/AB-JS) for higher *J* in terms of those for *J* = 0.

The presumably more accurate quantum mechanical method used to obtain rate coefficients, to which the results of these approximate methods are compared in the present article, is accurate quantum mechanics (QM) for *J* = 0 combined with *J*-shifting (QM/JS) to obtain higher *J* dynamics. In a more general context, a more accurate way to extend calculations at one or a few *J* values to all *J* is the separable rotation approximation (SRA)[24,25] based on results for *J* > 0, but in this paper, *J*-shifting is applied only to *J* = 0 results. Both *J*-shifting and the SRA (or, in the terminology of Nobusada and Nakamura, the "extended *J*-shift approximation") were tested recently[26] against accurate quantum calculations for the O(^{3}P) + HCl reaction using the potential energy surface obtained by Koizumi, Schatz, and Gordon[6] (KSG), and both approximations were found to be accurate to within 20% or better over a temperature range of 200−800 K. On the basis of these tests and the fact that the results in ref 1 agree with QM/JS results of Nobusada et al. on the same PES[9] within 20% over the 300−1000 K temperature range, one might assume that the results of ref 1 are accurate to better than a factor of 1.5 for the S4 potential and, in that sense, they serve as the benchmark against which the approximate methods mentioned above are tested.

The remainder of this paper is organized as follows. In the following section, we briefly describe each of the methods mentioned above. We also include in section II a discussion of the special difficulties posed by the O(^{3}P) + HCl reaction for the VTST and semiclassical tunneling methods, which require estimating accurate generalized transition state partition coefficients and effective tunneling potentials. In section III, we present the results of the dynamics calculations and discuss their implications. Section IV presents new electronic structure calculations of the saddle point properties. Finally, we conclude in section V with a summary of the present article and a discussion of its implications.

II. Methods

II.A. Quasiclassical Trajectory Method. The quasiclassical trajectory (QCT) method has been a workhorse of gas-phase reaction dynamics for a long time. A complete description of the QCT method has been given elsewhere,[10] and detailed studies of the reliability or unreliability of QCT methods in the context of elementary gas-phase reactions have been conducted.[27-32] The QCT calculations of the present work were used to obtain initial-rovibrational-state-selected reaction cross sections $\sigma_{vj}(E_{rel})$ as a function of the relative translational energy E_{rel}, where v is initial vibrational quantum number and j is initial rotational quantum number, from which the vibrational-state-selecteded rate coefficients $k_v(T)$ and thermal rate coefficients $k(T)$ were obtained by standard procedures.[10]

II.B. Transition State Theory and Variational Transition State Theory. Conventional[10,14,15,33] and variational[12-15,33] transition state theory (denoted TST and VTST, respectively) will both be used in this paper. In particular, we will use VTST in the form of the improved canonical variational theory (ICVT), which is described elsewhere.[13,14] Therefore, we focus here on the special challenges posed by the S4 PES for TST and VTST methods. The two main issues here are (a) the accurate treatment of the bending energy levels and (b) the evaluation of the partition functions. The first issue concerns how well the analytical fit we use in the partition function calculation approximates the bending potential on the S4 surface; the second concerns how the bending energy levels are computed for that approximate potential.

The saddle point and minimum-energy path (MEP) are bent on the S4 surface (bond angle 131°, i.e., about 50° from collinear), but the double-well bend potential is relatively shallow−only 3.18 kcal/mol if we straighten the saddle geometry and reoptimize bond lengths. (Note that 1 kcal/mol ≡ 4.184 kJ/mol.) There are two options for treating a nearly linear system: One can use a collinear reference path with a double-well bend potential, as has been implemented[34] in the ABCRATE computer code[35] with a quadratic-quartic bend potential, or one can use a nonlinear reference path. Although the former treatment is preferred for low barriers to collinearity,[34] in the present case, it is difficult to fit the entire bend potential (over the whole range from minimum to minimum) to a single quadratic-quartic potential (but the important region near the minima can be treated accurately by the WKB method). Furthermore, a very critical issue is that the harmonic frequency for the bound stretching frequency changes significantly in going from the collinear higher-order saddle point to the bent first-order saddle point (490 cm^{-1} versus 1523 cm^{-1}). In light of the dominance of the bent region in the thermal average, it is better to do the harmonic analysis near the bottom of the bending well so that the stretch mode is better represented by harmonic frequencies along the bent MEP. The relatively large difference in stretch harmonic frequencies at the collinear and bent geometries is an indication of coupling between these modes which is neglected in the current VTST approaches. This is one aspect of the S4 PES that makes it difficult to treat. Nevertheless, it seems clear that the treatment using a noncollinear reference path is more reasonable for this case, and this is the approach we used. In particular the thermal rate coefficient calculations for the present paper were carried out with the POLYRATE program[16,36,37] using a nonlinear reference path, curvilinear internal coordinates,[16,38] and the harmonic approximation for the stretch and a nondegenerate bend. A possibly significant qualitative result that emerges from the collinear-reference-path calculations is that the collinear-reference treatment leads to a greatly increased contribution from large-curvature tunneling paths.

We found that the Euler integration method *without* stabilization[39] was the best method for calculating the MEP on the S4 surface, and our final results are calculated by this method with a reduced mass (scaling mass) of 1 amu and a fixed step size

2300 *J. Phys. Chem. A, Vol. 105, No. 11, 2001*

Skokov et al.

TABLE 1: Harmonic Vibrational Frequencies (cm^{-1}) on the S4 Surface

	stretch	other
reactant	2991	
reactant-valley well	2935	186,[a] 148
saddle	1523	290, 1619i
product-valley well	3518	978, 287
product	3738	

[a] Doubly degenerate.

of $2 \times 10^{-4}a_0$. (Note that $1a_0 = 1$ bohr $= 0.5292 \times 10^{-10}$ m.) The MEP has an entrance-valley well of depth 1.64 kcal/mol, a barrier of height 9.78 kcal/mol, and a product-valley well of depth 5.18 kcal/mol relative to reactants. The reactant valley well has a collinear configuration of the three-atom system while the barrier and the product valley well are at O—H—Cl angles of 131.6 and 80.4°, respectively. The zero-point-exclusive energy of reaction is −0.09 kcal/mol, and ΔH_0 (which includes zero-point energy) is equal to 0.96 kcal/mol. The vibrational frequencies at the five stationary points are given in Table 1.

The relative vibrationally adiabatic ground-state potential curve, $\Delta V_a^G(s)$, is defined by[13]

$$\Delta V_a^G(s) = V_{MEP}(s) + \epsilon^G(s) - \epsilon^G(s = -\infty) \quad (1)$$

where $V_{MEP}(s)$ and s are the potential energy (relative to reactants) and distance (relative to the saddle point) along the MEP, $\epsilon^G(s)$ is the ground-state energy of the bound modes (i.e., those transverse to the MEP), and the last term of (1) is the ground-state energy of reactants. The potential $\Delta V_a^G(s)$ peaks at 8.31 kcal/mol at $s = -0.08a_0$, where $V_{MEP}(s)$ is 9.60 kcal/mol as compared to values of ΔV_a^G and $V_{MEP}(s)$ of 8.21 and 9.78 kcal/mol, respectively at the saddle point ($s = 0$). Therefore, the variational transition state is at $s = -0.08a_0$ at $T = 0$ K. Using curvilinear coordinates,[16,38] as we do here, yields bound frequencies of 1702 and 313 cm^{-1} at $s = -0.08$ a_0, whereas the less physical rectilinear treatment[14] yields 1673 and 288 cm^{-1}. These differences become more pronounced for locations farther from the transition state. For example, at $s = -0.40a_0$, the curvilinear treatment gives 2546 and 444 cm^{-1}, whereas the rectilinear one gives 2511 and 353 cm^{-1}.

At finite temperature, we employed improved canonical variational theory (ICVT).[14,40] The variational transition state location varies from $s = -0.07a_0$ at 200 K to $-0.19a_0$ at 1500 K. At the latter location ΔV_a^G and V_{MEP} are 8.12 and 8.93 kcal/mol, respectively. Thus, at 1500 K, the dynamical bottleneck for a canonical ensemble is located before the saddle point at a dividing surface where the reaction-path energy is still 0.85 kcal/mol below the saddle.

We also calculated state-selected rate coefficients for HCl in the excited $v = 1$ state in which the bound stretch mode was adiabatically restricted to the first excited state along the portion of the reaction path prior to the first local maximum in the reaction-path curvature; this is called partial-reaction-path (PRP) adiabaticity in a previous paper,[41] and we will use the same notation here. In particular, these calculations employed improved canonical variational theory (ICVT) and are denoted ICVT-AS(PRP), where the last part of the acronym denotes adiabatic stretch over the partial reaction path. The general method used to perform these state-selected calculations has been described elsewhere.[41-47] For the $v = 1$ calculations we replaced the harmonic treatment of the stretch coordinate by a rectilinear state-selected treatment[14] using the WKB approxima-tion, as discussed elsewhere.[48] We also replaced the harmonic

approximation for the bend by using the WKB approximation in rectilinear coordinates for the ground bend level and the curvilinear[38] Morse I approximation[49] with a $D_e(min)$[14] value of 106.48 kcal/mol for excited bend levels.

It is well-known that the stretch cannot necessarily be assumed to be adiabatic over the full reaction path.[41] However, there is no good theory for precisely where to relax the adiabatic constraint. Thus the calculations presented here use the recom-mendation of ref 41, i.e., the location of the first local maximum in the curvature. These calculations have interest primarily as a model treatment and serve as a diagnostic of the extent of adiabaticity. It is not clear if the WKB approximation in rectilinear coordinates is adequate; studies with a collinear reference path showed a much greater increase in the rate coefficient on switching from a curvilinear Morse I stretch to a curvilinear WKB stretch than the bent-reference-path calcula-tions show for a switch from a curvilinear Morse I stretch to a rectilinear WKB stretch; furthermore the $v = 1$ calculations have the same complications due to mode coupling (discussed above) that the thermal rate coefficient calculations have.

We also present some calculations of the $J = 0$ cumulative reaction probability (CRP). The first such set of calculations is based on harmonic conventional TST without tunneling. The CRP is defined as the sum of all state-to-state reaction probabilities at a given total energy, and its approximation by TST is explained elsewhere.[50-52] The second set is discussed in section II.C.

II.C. Tunneling Contributions. For the thermal (i.e., non-state selected) reaction, tunneling was included by the micro-canonical optimized multidimensional tunneling (μOMT) ap-proximation.[17] In the present case, the ICVT/μOMT results were computed using the harmonic approximation for both the bound stretching mode and the nondegenerate bend. In the μOMT method, the larger of the centrifugal-dominant small-curvature adiabatic ground-state (CD-SCSAG) transmission coefficient[53,54] and the large-curvature ground-state version-3 (LCG3) transmis-sion coefficient[17,54] at each total energy is selected. The μOMT results agree very well with the CD-SCSAG ones for the present reaction on the S4 surface because the small-curvature tunneling paths dominate over large-curvature ones.

The tunneling contribution in the partial-reaction-path adiabatic-stretch approximation for the $v = 1$ reaction rate was estimated by the CD-SCSAG approximation. The results obtained by adding this tunneling approximation to the $v = 1$ ICVT-AS-(PRP) rate coefficients are denoted ICVT-AS(PRP)/SCT. The calculation of state-selected tunneling contributions is discussed further in previous papers.[41-47,55,56]

We also calculated the $J = 0$ CRP implied by the harmonic ICVT/μOMT calculation. Since the ICVT transition state depends on T, the CRP that it implies depends on T as well, but the dependence is slight so we only present the results calculated for $T = 300$ K. Let s^* denote the location of the ICVT transition state. Note that s^* depends on temperature. (It is this dependence on T that makes the CRP depend on T.) Let $\Delta V_a^G(s)$ denote the vibrationally adiabatic ground-state poten-tial curve relative to the classical energy of reactants, i.e.,

$$V_a^G(s) = \Delta V_a^G(s) + \epsilon^G(s = -\infty) \quad (2)$$

and let the maximum of $V_a^G(s)$ be denoted V^{AG}. Then the $J = 0$ CRP implied by the ICVT/μOMT calculation is

$$CRP = \sum_\alpha P(E - V_{MEP}(s) - \epsilon_\alpha^{ICVT} + V^{AG}) \quad (3)$$

The O(^{3}P) + HCl Reaction

J. Phys. Chem. A, Vol. 105, No. 11, 2001 **2301**

TABLE 2: Thermal Rate Coefficients (cm^3 Molecule^{-1} s^{-1}) for the S4 Surface

T (K)	QCT	TST	ICVT	ICVT/μOMT	QM/AB-JS	QM/JS
250	2.5(−18)	1.1(−18)	8.7(−19)	1.8(−17)	5.4(−18)	1.2(−16)
298	2.6(−17)	1.6(−17)	1.3(−17)	1.1(−16)	2.0(−17)	4.8(−16)
300	2.9(−17)	1.8(−17)	1.4(−17)	1.2(−16)	2.0(−17)	5.1(−16)
400	6.8(−16)	5.9(−16)	4.9(−16)	1.5(−15)	3.1(−16)	4.2(−15)
600	1.9(−14)	2.2(−14)	1.9(−14)	3.1(−14)	7.1(−15)	5.2(−14)
800	1.1(−13)	1.5(−13)	1.3(−13)	1.7(−13)	3.7(−14)	2.1(−13)
1000	3.3(−13)	5.1(−13)	4.2(−13)	5.1(−13)	1.0(−13)	5.1(−13)

where $P(E)$ is the ground-state μOMT transmission probability at energy E and ϵ_α^{ICVT} is the αth energy level of the generalized transition state at s^*. One calculates the energy levels as a function of the two vibrational quantum numbers and then puts them in increasing order to get the list of ϵ_α^{ICVT} values. Note that the transmission probability and, therefore, the CRP vanishes for $E < E_0$, where E_0 is the greater of the ground-state energies of the reactants and products. For the S4 surface, $E_0 = 5.34$ kcal/mol, the zero-point energy of OH + Cl.

II.D. Reduced-Dimensionality Quantum Mechanical Calculations. The reduced-dimensionality-adiabatic-bend approach used here (denoted QM/AB for $J = 0$ and QM/AB-JS when extended to all J as explained in section I) has been described in detail elsewhere,[20] so we only give a brief description of it here along with details relevant for the present application. In this approach the two radial degrees of freedom are treated by a fully coupled quantum reactive scattering approach for zero total angular momentum. The remaining angular degree of freedom is treated adiabatically. The potential governing the reduced dimensionality two-degree-of-freedom dynamics is an effective potential given by the sum of a minimized three-degree-of-freedom potential plus the local adiabatic bend energy. In the present case, the S4 potential was minimized with respect to the OHCl bond angle, θ, for fixed values of the r_{OH} and r_{HCl} bond lengths. At each point in the two-dimensional (r_{OH}, r_{HCl}) space, the local bending frequency, $\omega_b(r_{OH}, r_{HCl})$, was determined as follows. The standard 3×3 G-matrix[57] was calculated and inverted, and the diagonal element $(G^{-1})_{\theta,\theta}$ was used together with $V_{\theta,\theta}$, the second derivative of the potential with respect to θ to determine $\omega_b(r_{OH}, r_{HCl})$ from the equation

$$\omega_b(r_{OH}, r_{HCl}) = \sqrt{\frac{V_{\theta,\theta}}{(G^{-1})_{\theta,\theta}}} \quad (4)$$

This approach is not exactly equivalent to performing a constrained normal-mode analysis; however, the resulting bend frequency at the saddle point, 260 cm^{-1}, is in good agreement with normal mode result of 290 cm^{-1}.

The reduced-dimensionality scattering calculations are done in Jacobi coordinates r (the HCl bond length) and R (the distance of O to the center of mass of HCl) for $J = 0$ with the Hamiltonian

$$H = T_r + T_R + V_{min}(r, R) + \hbar\omega_b(r, R)(n_b + 1/2) \quad (5)$$

where T_r and T_R are the usual radial kinetic energy operators, V_{min} is the minimized potential, and the last term is the local adiabatic bending energy for the bend state n_b. The transformation from bond lengths in eq 4 to Jacobi coordinates in eq 5 was done using collinear kinematics although the saddle point is bent. The two-dimensional time-dependent Schrödinger equation in r and R was solved using the recently developed L^2 method with damping.[58] This method has been described and tested previously for the three-dimensional D + H$_2$ reaction[58] and has also been applied previously to the O + HCl reaction.[1]

For the present work, the reduced-dimensionality L^2 calculations were carried out using a basis of 6500 eigenstates of the Hamiltonian given by eq 5 for the ground bend state, spanning a range in R from 3.0 to 12.5a_0 and in r from 1.5 to 9.0a_0. Calculations were also carried out with smaller bases to test the convergence of the results. These calculations yield the total reaction probability for $J = 0$ for various initial vibrational quantum numbers v of HCl and for the ground bend state quantum numbers n_2 of the three-atom system as a function of the total energy E. If we denote this probability by $P_v(E; n_2 = 0)$ then, as shown in detail elsewhere,[22] the CRP for $J = 0$ is given approximately by

$$N^{J=0} = \sum_v [P_v(E; n_2 = 0) + \sum_{n_2=1} P_v(E - n_2 hc\omega_2; n_2 = 0)] \quad (6)$$

where ω_2 is the bend frequency of the transition state. One includes as many terms in the sum as are required for convergence. Then by application of J-shifting to the $J = 0$ CRP (as was done to the exact CRP in eq 3 of ref 1), the full CRP can be obtained in the J-shifting approximation, and from it the thermal rate coefficient, as given in detail in ref 1. The QM/AB-JS thermal rate coefficient was obtained using the saddle point harmonic bend frequency and rotation constants.

The initial state-selected rate coefficient for $v = 1$ is obtained following the above steps except that only the $v = 1$ term is included in eq 6. The QM/AB-JS results used the bend frequency (220 cm^{-1}) of the variational transition state for $v = 1$ instead of the bend frequency of the saddle point (290 cm^{-1}).

II.E. Quantum Mechanical Calculations with J-Shifting. Another set of calculations was carried out in which the $J = 0$ dynamics was solved accurately in the full dimensionality by time-dependent wave packet propagation. These calculations are denoted as QM for $J = 0$ and QM/JS when extended to all J by the J-shifting approximation. Full details of these calculations are given in ref 1. The only difference between the reduced-dimensionality and full-dimensionality thermal and initial-vibrational-state-selected rate coefficient is in the CRP for $J = 0$.

III. Results and Discussion

III.A. Thermal Rate Coefficients. The thermal rate coefficients are given in Table 2. All rate coefficients in this article include the multiple-surface coefficient,[59] which is the degeneracy of the transition state (which is 3) divided by the electronic partition coefficient of the ^{3}P$_{2,1,0}$ states of O. For O(^{3}P) + HCl, this ratio varies from 0.46 at 250 K to 0.37 at 1000 K. The thermal rate coefficients are also presented in Figure 1. The QM/JS calculations in all tables and figures are from ref 1; they agree with the QM/JS results of ref 9, calculated using R-matrix propagation in hyperspherical elliptic coordinates,[60] within 11% at 300 K, 3% at 600 K, and 20% at 1000 K, and they will serve as a standard against which to compare the more approximate methods.
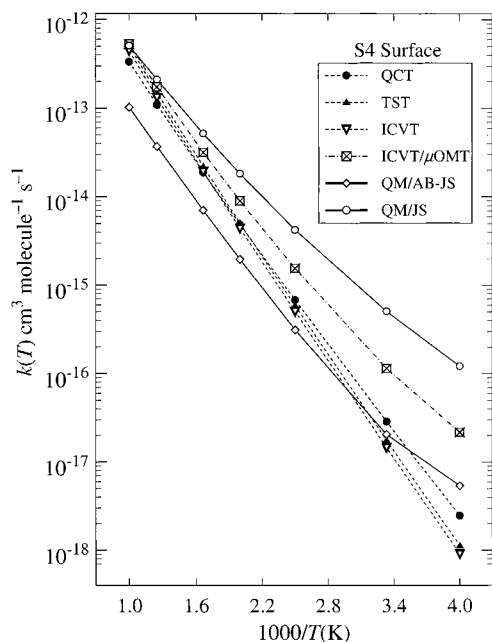
Figure 1. Thermal rate coefficients for the $O(^3P)$ + HCl reaction on the S4 potential energy surface.

Figure 2. Comparison of the QM/JS (solid smooth curve), QM/AB-JS (dashed curve), QCT (dot−dashed curve), ICVT/μOMT (triple-dot−dashed curve), and conventional transition state (solid stepped curve) cumulative reaction probabilities for $J = 0$ on the S4 PES. Note that the conventional TST result is based on the harmonic approximation for this figure; it includes quantized vibrations at the saddle point, but the reaction coordinate is treated classically. The ICVT/μOMT result also has quantized harmonic vibrations, and in addition, variational effects and tunneling are included.

The ICVT transition state is located at $s = -0.074a_0$ at 250 K (where the frequencies are 1687 and 311 cm^{-1}, the bond distances are 2.50 (OH) and 2.61a_0 (HCl), and the bond angle is 131°); at 1000 K, it is at $s = -0.122a_0$ (where the frequencies are 1813 and 327 cm^{-1}, the bond distances are 2.55 (OH) and 2.58a_0 (HCl), and the bond angle is 130°). It is seen that the QCT, TST, and ICVT results are reasonably close to each other (within a factor of 2.7) over the entire temperature range, and they are even closer at high temperature (a factor of 1.6 at 1000 K). The difference between the ICVT and ICVT/μOMT results indicates the magnitude of the semiclassical tunneling correction, which is significant at low temperature. As mentioned in section II.C, the large-curvature tunneling approximation gave smaller transmission coefficients than the small-curvature tunneling approximation; we have found in previous work that large-curvature tunneling sometimes but not always dominates for heavy-light-heavy bimolecular reactions. Given the importance of tunneling in a heavy-light-heavy reaction involving the exchange of a hydrogen atom with an appreciable barrier, it is not surprising that the QM/JS rate coefficients are significantly higher than those predicted by methods that do not include tunneling. The inclusion of semiclassical tunneling calculations in the ICVT/μOMT rate coefficients improves the situation but not as much as one expects from previous tests of this method against accurate quantum results. As discussed above, this reaction exhibits significant bend−stretch coupling, and it also probably has significant bend−rotation coupling; for these reasons we suspect that the separation of rotation from vibration and the separable-mode harmonic approximation are responsible for the larger than usual deviation of the ICVT/μOMT rate coefficients from the benchmark ones. Table 2 does not give CVT/μOMT rate coefficients, but they agree with the ICVT/μOMT rate coefficients within 2% over the temperature range shown.

The reduced dimensionality-adiabatic bend (QM/AB-JS) results lie below the ICVT/μOMT results over the entire range of temperatures examined. To elucidate the source of the errors in the QM/AB-JS calculations of the thermal rate coefficient we compare the QM and QM/AB CRPs for zero total angular momentum in Figure 2. For reference, the conventional har-
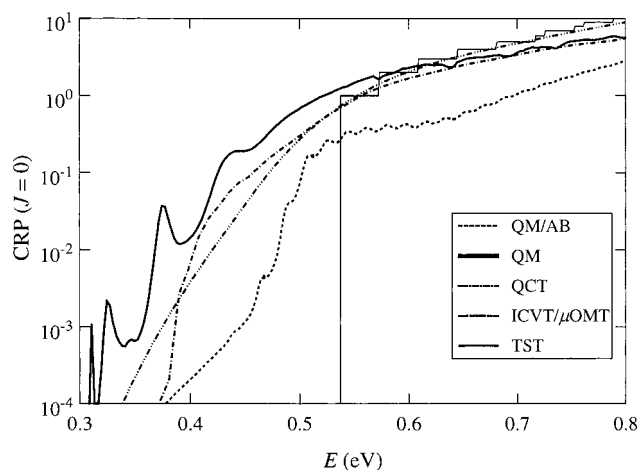
monic TST CRP and the $J = 0$ CRP implied by the harmonic ICVT/μOMT calculations are also plotted in this figure. As seen here, the QM CRP exhibits a highly structured dependence on E. This is especially prominent and significant for energies in the tunneling regime, and the figure shows that this structure is not found in the QM/AB calculations. The conventional harmonic TST CRP exceeds the exact one for $E > 0.6$ eV, and it is roughly a factor of 2 larger than at 0.8 eV. This indicates that recrossing of the conventional transition state and/or anharmonicity is very significant at these higher energies. ICVT corrects for recrossing at the saddle point by applying the no-recrossing assumption at the ICVT variational transition state; the ICVT/μOMT results are too low, probably (as discussed in the previous paragraph) because of the separable-mode character of the present treatment. The ICVT/μOMT results are, however, larger and more accurate than the QM/AB results; one possible reason for this is that the CD-SCSAG and μOMT approximations include corner cutting tunneling through the bend degree of freedom, whereas this is neglected in the QM/AB calculations. To test this, we repeated the ICVT/SCT calculations (which agree well with the ICVT/μOMT ones) with no corner cutting allowed in the bend coordinate. This reduces the predicted rate coefficient but by only 18% at 150 K and 12% at 298−300 K. Thus the effect is not large enough to be the dominant error in the QM/AB-JS calculations.

For both ICVT/μOMT and the adiabatic bend approximation, the deviations from the accurate CRP is larger than in previously studied atom−diatom systems with a simple barrier. Since the resonance structure in the accurate CRP is absent in the calculations that assume an adiabatic bend, these resonances may have something to do with the breakdown.

Table 3 and Figure 3 show the results for the KSG surface. The QCT results for this comparison have been taken from the work of Aoiz et al.,[61] the QM/JS results are from ref 1, and the remaining results are from computations performed for ref 8. There are several interesting differences between the behavior of the rate coefficients for the S4 and KSG surfaces. Once again, the QCT, TST, and ICVT results are in good agreement with each other at low temperature, but the TST and ICVT results are much higher than the QCT results at higher temperatures.

TABLE 3: Thermal Rate Coefficients (cm³ Molecule⁻¹ s⁻¹) for the KSG Surface

T (K)	QCT[51]	TST	ICVT	ICVT/μOMT	QM/JS
250	na[a]	1.3(−17)	7.1(−18)	3.3(−17)	8.0(−17)
298	na[a]	1.2(−16)	7.2(−17)	2.1(−16)	4.0(−16)
300	8.7(−17)	1.3(−16)	7.8(−17)	2.3(−16)	4.1(−16)
400	1.2(−15)	2.4(−15)	1.6(−15)	3.0(−15)	3.6(−15)
600	1.6(−14)	4.9(−14)	3.7(−14)	4.8(−14)	3.9(−14)
800	na[a]	2.4(−13)	1.9(−13)	2.2(−13)	1.5(−13)

^{a} Not available.
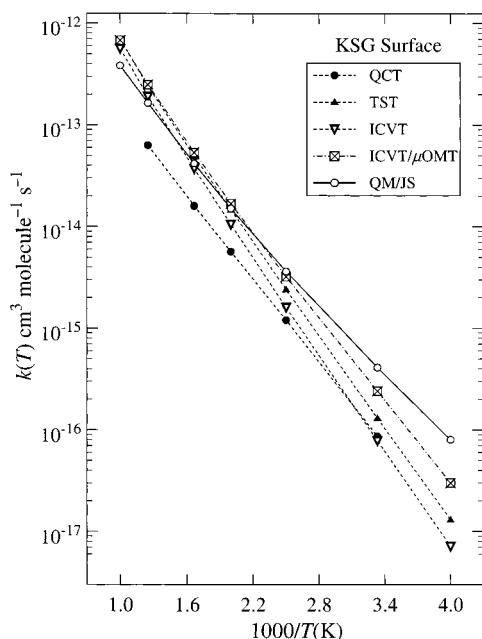
Figure 3. Thermal rate coefficients for the O(^{3}P) + HCl reaction on the KSG PES. Note that the QCT results (taken from ref 59) extend only from 300 to 600 K.

In fact, the ICVT results are higher than the QCT results by a factor of 2.3 at 600 K. At 1000 K, the ICVT rate coefficients are larger than the QM/JS ones by a factor of 1.65, which is larger than the more typical overestimate[19] of a factor of 1.2−1.3 at this temperature. In contrast to the results on the S4 surface, however, the ICVT/μOMT and QM/JS results on the KSG surface are in reasonably good agreement with each other, agreeing within a factor of 2.4 over the entire temperature range. It is also noteworthy that the difference between the ICVT and ICVT/μOMT rate coefficients are smaller on the KSG surface than the S4 surface at every temperature examined, indicating that the effective barrier on the KSG surface permits less tunneling than that on the S4 surface.

Experimental measurements of thermal rate coefficients for the O(^{3}P) + HCl reaction[62−72] span the temperature range of 293−1480 K. These values agree almost perfectly with the ICVT/μOMT curve for the S4 surface in Figure 1. However, since the QM/JS results on both the S4 and KSG surfaces lie above the experimental curve, it appears that this good agreement results from a cancellation of errors between those due to the potential energy surface and those due to the ICVT/μOMT dynamics.

One further aspect of the thermal rate constants that merits discussion is the phenomenological Arrhenius activation energy E_a. This was calculated from several of the sets of theoretical or experimental rate constants by fitting the thermal rate coefficients at two temperatures T_1 and T_2 to the expression

$$k(T) = Ae^{-E_a/RT} \qquad (7)$$

TABLE 4: Arrhenius Parameters for the Calculated and Experimental Thermal Rate Coefficients

T (K)	A (cm³ molecule⁻¹ s⁻¹)	E_a (kcal/mol)
	S4 Surface	
QCT	1.5(−11)	7.9
TST	3.4(−11)	8.6
ICVT	3.1(−11)	8.7
ICVT/μOMT	1.3(−11)	6.9
QM/AB-JS	3.4(−12)	7.2
QM/JS	7.8(−12)	5.7
	KSG Surface	
TST	2.9(−11)	7.2
ICVT	2.1(−11)	7.4
ICVT/mOMT	1.4(−11)	6.6
QM/JS	5.2(−12)	5.6
	Experiment	
ref. 68	8.6(−11)	6.4
ref. 72	7.4(−12)	6.4

and the results are summarized in Table 4. For the calculated results, the temperatures used are $T_1 = 300$ K and $T_2 = 800$ K. For the experimental results, $T_1 =$ the lowest temperature at which experimental results were reported and $T_2 =$ lower of the highest temperature at which experimental results were reported and 800 K. (This yields a T range of 293−718 K for ref 68 and a T range of 350−800 K for ref 72.) Table 4 shows that the QCT, TST, and ICVT results, none of which include tunneling, give fairly high energies of activation for the S4 surface, in the range 7.9−8.7 kcal/mol, whereas the ICVT/μOMT, QM/AB-JS, and QM/JS methods, which all do include tunneling, give energies of activation that are about 2 kcal/mol lower, in particular 5.7−7.2 kcal/mol. A tunneling effect of this magnitude is not too unusual for a hydrogen atom transfer reaction. The tunneling effect is smaller, only about 1 kcal/mol, for the KSG surface. Trying to decide which surface is preferred on the basis of E_a alone can be very misleading and is particularly impossible in the present case since the ICVT/μOMT activation energies for both surfaces agree with both sets of experimental results within their experimental uncertainties.

III.B. State-Selected Rate Coefficients. Table 5 and Figure 4 present QCT, adiabatic-stretch (partial-reaction-path) variational transition state theory, and QM/AB-JS results for $v = 1$. It is clear from Table 5 and Figure 4 that there are significant differences between the QCT and ICVT results, in contrast to the case of the thermal rate coefficients. The conventional TST results are not given but would be very large. An examination of the vibrationally adiabatic potentials for the $v = 0$ and $v = 1$ states, presented in Figure 5, helps to elucidate this behavior. If the stretch is adiabatic over the full reaction path, the dynamical-bottleneck for $k_{v=1}(T)$ is located in the entrance valley at all temperatures. On the other hand, the TST results would be evaluated using the classical barrier height and partition functions *at the saddle point*. The difference between the ICVT and the ICVT-AS/SCT rate coefficients is a measure of the semiclassically calculated contribution for tunneling through the effective barrier, which is shown in Figure 5 and is broader than that for the $v = 0$ case. As a result of this broadness, if the transmission coefficients were calculated under the assumption of full-reaction-path stretch adiabaticity, they would be significantly smaller than the values actually obtained, which range from 9.9 at 250 K to 1.7 at 1000 K. Even after inclusion of these tunneling contributions, though, the PRP adiabatic stretch rate coefficients are too small, by factors of 9−10 at 250−300 K, 5 at 400 K, and 3 at 500 K. The fact that the deviations are significantly larger than for ICVT/SCT calculations on the

TABLE 5: State-Selected Rate Coefficients $k_{v=1}(T)$ for the S4 Surface

T (K)	QCT	ICVT-AS(PRP)	ICVT-AS(PRP)/SCT	QM/AB-JS	QM/JS
250	1.8(−14)	3.0(−16)	3.0(−15)	6.3(−14)	4.0(−14)
298	4.4(−14)	1.7(−15)	8.4(−15)	1.1(−13)	7.9(−14)
300	4.5(−14)	1.8(−15)	8.7(−15)	1.1(−13)	8.1(−14)
400	1.5(−13)	1.8(−14)	4.2(−14)	2.3(−13)	2.2(−13)
500	3.5(−13)	7.4(−14)	1.3(−13)	3.9(−13)	4.3(−13)
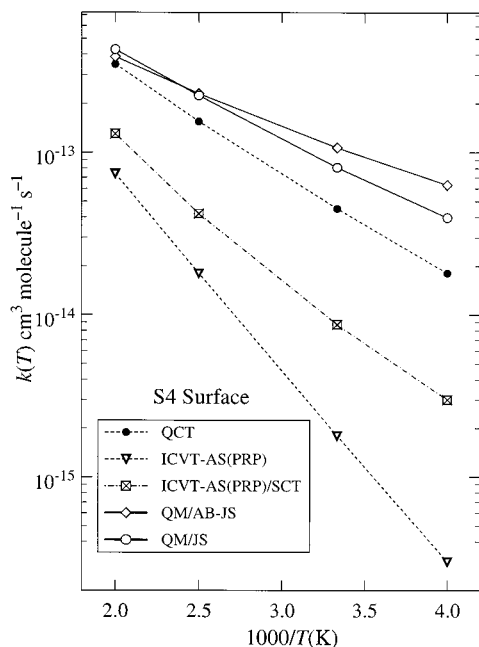
Figure 4. Rate coefficients for the $O(^3P)$ + HCl($v = 1$) reaction on the S4 PES.
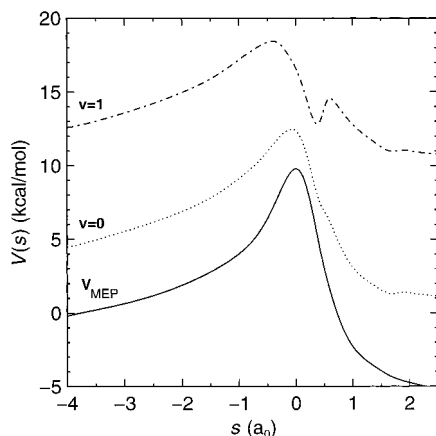
Figure 5. Potential along the minimum energy path (MEP) and the vibrationally adiabatic potentials for $v = 0$ and $v = 1$ states on the S4 PES. For this figure, the vibrational energies of both the stretch and the bend are calculated by the Morse I approximation.

thermal rate coefficient provides useful physical information about the state-selected reaction; in particular, it indicates that the assumption of stretch adiabaticity all the way up to the state-selected variational transition state may be invalid. We have seen the effect of vibrational nonadiabaticity of even high-frequency modes in previous work on the O + H$_2$ and H + OH reactions,[41] although in previous cases the breakdown appears to have occurred relatively later. The QCT results are more accurate than the ICVT results, but the QCT results are not expected to be reliable for $v = 1$ because they do not retain the quantization effects even when the system is quantum mechanically vibrationally adiabatic; the good agreement of the QCT results for $v = 1$ with the accurate results may be due to
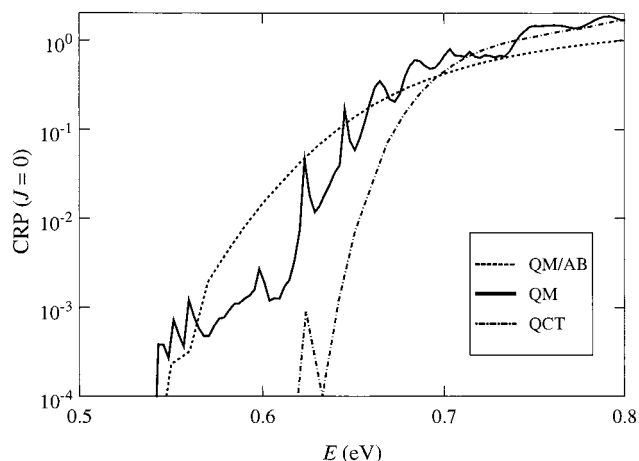
Figure 6. QM (solid line), QM/AB (dashed line) and QCT (dot-dashed line) cumulative reaction probabilities for $v = 1$ on the S4 PES.

a cancellation between excessive nonadiabatic leak and neglect of tunneling.

The QM/AB-JS rate coefficient for $v = 1$ is in good agreement with the QM/JS one. This agreement contrasts to the comparison for the thermal rate coefficient (which is dominated by the $v = 0$ contribution over the temperature range considered). To investigate this we compare the QM/AB and QM CRPs for $v = 1$ and $J = 0$ in Figure 6. The QM CRP is highly structured, whereas the QM/AB one is monotonically increasing with E. However, unlike the full CRP for $J = 0$, the QM/AB one is roughly the average of the accurate CRP for $v = 1$.

Experimental measurements of vibrational state selected rate coefficients[73−77] are complicated by the rapid relaxation of the $v = 1$ state of HCl. Therefore, most experiments directly measure the total rate of disappearance of HCl($v = 1$), both due to vibrational relaxation and reaction. However, Kneba and Wolfrum[77] report an absolute rate coefficient of 6.4 × 10^{-14} cm^3 molecule s^{-1} for $O(^3P)$ + HCl($v = 1$) → OH($v = 0$) + Cl($^2P_{3/2}$, $^2P_{1/2}$) at 298 K. This is in good agreement with the QM/JS value of $k_{v=1}(T)$ given in Table 5. The QM/JS rate coefficients on the S4 surface are larger than the experimental value by only about 23%.

IV. Electronic Structure Calculations

The saddle point geometry ($r^{\ddagger}_{OH}$, $r^{\ddagger}_{HCl}$, and $\theta^{\ddagger}_{OHCl}$) and barrier height ($V^{\ddagger}$) of the S4 surface are given in Table 6, in the row corresponding to $s = 0$. Since the most accurate available quantum mechanical rate coefficients for this surface are larger than experiment, it is interesting to carry out additional electronic structure calculations to explore the convergence of the saddle point properties.

Although the cc-pVTZ basis used for the S4 surface is very good for first-row elements, it suffers from insufficient spanning of the tight d space. This deficiency is corrected in the modified G3 large basis set (denoted MG3), which is used in the Multi-Coefficient Gaussian-3 method (denoted MCG3).[78] The

The O(^{3}P) + HCl Reaction

J. Phys. Chem. A, Vol. 105, No. 11, 2001 **2305**

TABLE 6: Single-Point Calculations of the Energy along the S4 Reaction Path

s (bohr)	geometry[a]			V_{MEP} (kcal/mol)		
	$r_{OH}^{\ddagger}$	$r_{HCl}^{\ddagger}$	$\theta_{OHCl}^{\ddagger}$	S4	MCG3-v2s	MCG3-v2 m
$-\infty^b$	∞	2.411		0.00	0.00	0.00
-0.80	3.168	2.423	115.9	4.73	5.50	5.37
-0.40	2.823	2.460	124.7	7.19	7.87	7.77
0	2.424	2.664	131.6	9.78	9.65	9.56
0.44	2.014	3.051	130.5	4.06	6.95	6.67
0.74	1.913	3.336	120.8	-0.18	3.47	3.11
0.84	1.905	3.428	117.1	-1.16	2.54	2.31
∞^c	1.827	∞		-0.09	-0.38	0.07

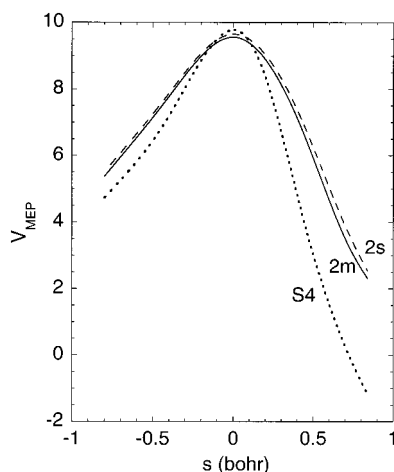[a] Distances in bohrs, angles in deg. [b] O + HCl. [c] OH + Cl.

Figure 7. Potential energy (kcal/mol) along the S4 MEP. Three values are shown: the S4 surface itself (dotted curve); MCG3-v2m calculations (solid curve); MCG3-v2s calculations (dashed curve).

MCG3 method includes an extrapolation to an infinite basis one-electron basis set and an infinite-order treatment of the many-electron correlation energy.[78,79] In the present paper we use versions 2s[80] and 2m[81] of the MCG3 method.

MCG3 calculations were carried out for 6 points on the S4 MEP, including the S4 saddle point. The results are given in Table 6 and Figure 7, where all energies are relative to reactants. We see that the MCG3 calculations are not sensitive to the choice of version number (the versions represent two different ways to parametrize the theory; version 2s includes spin−orbit effects explicitly, while version 2m includes them implicitly). Furthermore, the predicted energy relative to reactants at the S4 barrier is in excellent agreement with the S4 value. However, the MCG3 calculations clearly lead to a somewhat wider barrier, which would lead to less tunneling. Recent calculations by Peterson and one of the authors[82] at the MRCI+Q/CBS level of theory, using basis sets and extrapolation methods identical to those used for a recent highly accurate potential surface for HOCl,[83] also yield a broader reaction barrier than that of the S4 surface. However, the barrier heights predicted by these calculations are slightly higher than that of the S4 surface. Therefore, it seems safe to conclude that the S4 barrier is certainly too thin but there is still some uncertainty as to the correct barrier height.

V. Concluding Remarks

On the basis of the comparison of the quantum mechanical calculations using *J*-shifting to experiment, it appears that the S4 surface barrier is either too low or too "thin" or both. New electronic structure calculations by the MCG3 method point to the latter possibility; i.e., the S4 barrier is too thin. One can often gain a better understanding of which regions of the potential energy surface are most significant by examining semiclassical calculations of the rate coefficient, but the errors in the semiclassical calculations appear to be larger than usual in the present case. Further work is required to understand this since semiclassical and quantal results agree much better for the KSG surface for this reaction as well as for other systems. The most plausible explanation is that the effective potential for tunneling and/or overbarrier dynamics on the S4 surface is very sensitive to bend−stretch and bend−rotation coupling, which were not included in the VTST or semiclassical tunneling calculations. For example, since we found that the large-curvature tunneling is sensitive to the treatment of the bend, we may question whether a more accurate treatment of the bend could increase the large-curvature tunneling contributions relative to the small-curvature and overbarrier ones. This possibility makes the present reaction particularly interesting for further study. The results obtained by the adiabatic bend approximation are also interesting. The adiabatic bend calculations treat two of the internal degrees of freedom quantum mechanically, but the bend coordinate is assumed to be adiabatic and is not available for corner-cutting tunneling. This leads to worse agreement than ICVT/μOMT with the fully quantum mechanical calculations, although a test showed that this is apparently not due to neglect of corner cutting in the bend coordinate which is neglected in the adiabatic bend calculations but not in ICVT/μOMT. Another possibility is that the larger values of the QM/JS rate coefficients could be due to the dominance, in the full dimensional quantum calculations, of resonances associated with the bending motion which are not included in the ICVT/μOMT or reduced-dimensionality adiabatic-bend methods.

For the state-selected rate coefficients, the adiabatic-bend treatment is more accurate than the model that assumes that the stretch mode is adiabatic along the reaction path up to the first local maximum in the reaction path curvature, indicating that nonadiabaticity may set in a little earlier.

References and Notes

(1) Skokov, S.; Tsuchida, T.; Nanbu, S.; Bowman, J. M.; Gray, S. K. *J. Chem. Phys.* **2000**, *113*, 227.

(2) Ramachandran, B.; Schrader, E. A., III; Senekowitsch, J.; Wyatt, R. E. *J. Chem. Phys.* **1999**, *111*, 3862.

(3) Brown, F. B.; Truhlar, D. G. *Chem. Phys. Lett.* **1985**, *117*, 307.

(4) Ramachandran, B. *J. Chem. Phys.* **2000**, *112*, 3680.

(5) Zhang, R., van der Zande, W. J., Bronikowski, M. J., Zare, R. N. *J. Chem. Phys.* **1991**, *94*, 2704.

(6) Koizumi, H.; Schatz, G. C.; Gordon, M. S. *J. Chem. Phys.* **1991**, *85*, 6421.

(7) Ramachandran, B., Senekowitsch, J., Wyatt, R. E. *Chem. Phys. Lett.* **1997**, *270*, 387.

(8) Allison, T. C.; Ramachandran, B.; Senekowitsch, J.; Truhlar, D. G.; Wyatt, R. E. *J. Mol. Struct.* (*Theochem*) **1998**, *454*, 307.

(9) Nobusada, K.; Nakamura, H.; Lin, Y.; Ramachandran, B. *J. Chem. Phys.* **2000**, *113*, 1018.

(10) Truhlar, D. G.; Muckerman, J. M. In *Atom-Molecule Collision Theory: A Guide for the Experimentalist*; Bernstein, R. B., Ed.; Plenum: New York, 1979; pp 505−566.

(11) Glasstone, S.; Laidler, K.; Eyring, H. *The Theory of Rate Processes*; McGraw-Hill: New York, 1941.

(12) (a) Garrett, B. C.; Truhlar, D. G. *J. Phys. Chem.* **1979**, *83*, 1052. (b) Garrett, B. C.; Truhlar, D. G.; Grev, R. S. In *Potential Energy Surfaces and Dynamics Calculations*; Truhlar, D. G., Ed.; Plenum: New York, 1980; pp 587−637.

(13) (a) Garrett, B. C.; Truhlar, D. G.; Grev, R. S.; Magnuson, A. W. *J. Phys. Chem.* **1980**, *84*, 1730; **1983**, *87*, 4554 (E). (b) Isaacson, A. D.; Truhlar, D. G. *J. Chem. Phys.* **1982**, *76*, 1380.

(14) Truhlar, D. G.; Isaacson, A. D.; Garrett, B. C. In *Theory of Chemical Reaction Dynamics*; Baer M., Ed.; CRC Press: Boca Raton, FL, 1985; Vol. 4, pp 65−137.

(15) Tucker, S. C.; Truhlar, D. G. In *New Theoretical Concepts for Understanding Organic Reactions*; Bertrán, J., Csizmadia, I. G., Eds.; NATO ASI Series C267; Kluwer: Dordrecht, The Netherlands, 1989; pp 291−346.

(16) Chuang, Y.-Y.; Corchado, J. C.; Fast, P. L.; Villà, Hu, W.-P.; Liu, Y.-P.; Lynch, G. C.; Jackels, C. F.; Nguyen, K. A.; Gu, M. Z.; J.; Rossi, I.; Coitiño, E. L.; Clayton, C.; Melissas, V. S.; Lynch, B.; Steckler, R.; Garrett, B. C.; Isaacson, A. D.; Truhlar, D. G. *Polyrate-Version 8.4.1*; University of Minnesota: Minneapolis, MN, 1998.

(17) Liu, Y.-P.; Lu, D.-h.; González-Lafont, A.; Truhlar, D. G.; Garrett, B. C. *J. Am. Chem. Soc.* **1993**, *115*, 7806.

(18) Truhlar, D. G.; Garrett, B. C.; Klippenstein, S. J. *J. Phys. Chem.* **1996**, *100*, 12771.

(19) Allison, T. C.; Truhlar, D. G. In *Modern Methods for Multidimensional Dynamics Computations in Chemistry*; Thompson, D. L., Ed.; World Scientific: Singapore, 1999; pp 618−712.

(20) Bowman, J. M. *Adv. Chem. Phys.* **1985**, *61*, 115.

(21) Bowman J. M.; Wang, D.-S. In *Advances in Molecular Vibrations and Collision Dynamics*; Bowman, J. M., Ed.; JAI: Greenwich, 1994; Vol IIB, pp 187−223.

(22) Bowman, J. M.; Wagner, A. F. In *The Theory of Chemical Reaction Dynamics*; Clary, D. C., Ed.; NATO ASI Series C170; Reidel: Dordrecht, The Netherlands, 1986; pp 47−76.

(23) Bowman, J. M. *J. Phys. Chem.* **1991**, *95*, 4960.

(24) Mielke, S. L.; Lynch, G. C.; Truhlar, D. G.; Schwenke, D. W. *Chem. Phys. Lett.* **1993**, *216*, 441.

(25) Mielke, S. L.; Lynch, G. C.; Truhlar, D. G.; Schwenke, D. W. *J. Phys. Chem.* **1994**, *98*, 8000.

(26) Nobusada, K.; Nakamura, H. *J. Phys. Chem. A* **1999**, *103*, 6715.

(27) Truhlar, D. G. *J. Phys. Chem.* **1979**, *83*, 188.

(28) Zhao, M.; Mladenovic, M.; Truhlar, D. G.; Schwenke, D. W.; Sun, Y.; Kouri, D. J.; Blais, N. C. *J. Am. Chem. Soc.* **1989**, *111*, 852.

(29) Blais, N. C.; Zhao, M.; Mladenovic, M.; Truhlar, D. G.; Schwenke, D. W.; Sun, Y.; Kouri, D. J. *J. Chem. Phys.* **1989**, *91*, 1038.

(30) Blais, N. C.; Zhao, M.; Truhlar, D. G.; Schwenke, D. W.; Kouri, D. J. *Chem. Phys. Lett.* **1990**, *166*, 11; **1992**, *188*, 368 (E).

(31) Keogh, W. J.; Boothroyd, A. I.; Martin, P. G.; Mielke, S. L.; Truhlar, D. G.; Schwenke, D. W. *Chem. Phys. Lett.* **1992**, *195*, 144.

(32) Aoiz, F. J.; Bañares, L.; Herrero, V. J. In *Advances in Classical Trajectory Methods*; Hase, W. L., Ed.; JAI: New York, 1998; Vol. 3 and references therein.

(33) Kreevoy, M.; Truhlar, D. G. In *Investigation of Rates and Mechanisms of Reaction*; Techniques of Chemistry, 4th ed., Vol. 6; Bernasconi, C. F., Ed.; John Wiley & Sons: New York, 1986; Part 1, pp 13−95.

(34) Garrett, B. C.; Truhlar, D. G.; Wagner, A. F.; Dunning, T. H., Jr. *J. Chem. Phys.* **1983**, *78*, 4400.

(35) Garrett, B. C.; Lynch, G. C.; Allison, T. C.; Truhlar, D. G. *Comput. Phys. Commun.* **1998**, *109*, 47.

(36) Steckler, R.; Hu, W.-P.; Liu, Y.-P.; Lynch, G. C.; Garrett, B. C.; Isaacson, A. D.; Melissas, V. S.; Lu, D.-h.; Truong, T. N.; Rai, S. N.; Hancock, G. C.; Lauderdale, J. G.; Joseph, T.; Truhlar, D. G. *Comput. Phys. Commun.* **1995**, *88*, 341.

(37) Lu, D.-h.; Truong, T. N.; Melissas, V. S.; Lynch, G. C.; Liu, Y.-P.; Garrett, B. C.; Steckler, R.; Isaacson, A. D.; Rai, S. N.; Hancock, G. C.; Lauderdale, J. G.; Joseph, T.; Truhlar, D. G. *Comput. Phys. Commun.* **1992**, *71*, 235.

(38) Nguyen, K. A.; Jackels, C. F.; Truhlar, D. G. *J. Chem. Phys.* **1996**, *104*, 6491.

(39) Melissas, V. S.; Truhlar, D. G.; Garrett, B. C. *J. Chem. Phys.* **1992**, *96*, 5758.

(40) Isaacson, A. D.; Sund, M. T.; Rai, S. N.; Truhlar, D. G. *J. Chem. Phys.* **1985**, *82*, 1338.

(41) Garrett, B. C.; Truhlar, D. G.; Bowman, J. M.; Wagner, A. F. *J. Phys. Chem.* **1986**, *90*, 4305.

(42) Truhlar, D. G.; Issacson, A. D. *J. Chem. Phys.* **1982**, *77*, 3516.

(43) Garrett, B. C.; Truhlar, D. G. *J. Chem. Phys.* **1984**, *81*, 309.

(44) Garrett, B. C.; Truhlar, D. G. *J. Phys. Chem.* **1985**, *89*, 2204.

(45) Garrett, B. C.; Truhlar, D. G. *Int. J. Quantum Chem.* **1986**, *29*, 1463.

(46) Garrett, B. C.; Truhlar, D. G.; Varandas, A. J. C.; Blais, N. C. *Int. J. Chem. Kinet.* **1986**, *18*, 1065.

(47) Steckler, R.; Truhlar, D. G.; Garrett, B. C. *J. Chem. Phys.* **1986**, *84*, 6712.

(48) Hancock, G. C.; Rejto, P. A.; Steckler, R.; Brown, F. B.; Schwenke, D. W.; Truhlar, D. G. *J. Chem. Phys.* **1986**, *85*, 4997.

(49) Garrett B. C.; Truhlar, D. G. *J. Phys. Chem.* **1979**, *83*, 1079; **1980**, *84*, 682 (E); **1983**, *87*, 4553 (E).

(50) Miller, W. H. *J. Chem. Phys.* **1975**, *62*, 1899.

(51) Miller, W. H. In *Potential Energy Surfaces and Dynamics Calculations*; Truhlar, D.G., Ed.; Plenum: New York, 1981; pp 265−286.

(52) Chatfield, D. G.; Friedman, R. S.; Truhlar, D. G.; Garrett, B. C.; Schwenke, D. W. *J. Am. Chem. Soc.* **1991**, *113*, 486.

(53) Liu, Y.-P.; Lynch, G. C.; Truong, T. N.; Lu, D.-h.; Truhlar, D. G. *J. Am. Chem. Soc.* **1993**, *115*, 2408.

(54) Truong, T. N.; Lu, D.-h.; Lynch, G. C.; Liu, Y.-P.; Melissas, V. S.; Stewart, J. J. P.; Steckler, R.; Garrett, B. C.; Isaacson, A. D.; González-Lefont, A.; Rai, S. N.; Hancock, G. C.; Joseph, T.; Truhlar, D. G. *Comput. Phys. Commun.* **1993**, *75*, 143.

(55) Garrett, B. C.; Abusalbi, N.; Kouri, D. J.; Truhlar, D. G. *J. Chem. Phys.* **1985**, *83*, 2252.

(56) Garrett, B. C.; Truhlar, D. G.; Varandas, A. J. C.; Blais, N. C. *Int. J. Chem. Kinet.* **1986**, *18*, 1065.

(57) Wilson, E. B., Jr.; Decius, J. C.; Cross, P. C. *Molecular Vibrations*; Dover: New York, 1955.

(58) Skokov, S.; Bowman, J. M. *Phys. Chem. Chem. Phys.* **2000**, *2*, 495.

(59) Truhlar, D. G. *J. Chem. Phys.* **1972**, *56*, 3189; **1974**, *61*, 440 (E).

(60) Tolstikhin, O. I.; Nakamura, H. *J. Chem. Phys.* **1998**, *108*, 8899. Nobusada, K.; Tolstikhin, O. I.; Nakamura, H. *J. Chem. Phys.* **1998**, *108*, 8922.

(61) Aoiz, F. J.; Banares, L.; Castillo, J. F.; Menendez, M.; Verdasco, J. E. *Phys. Chem. Chem. Phys.* **1999**, *1*, 1149.

(62) Balakhnin, V. P.; Egorov, V. I.; Interzarova, E. I. *Kinet. Katal.* **1971**, *12*, 255; **1971**, *12*, 298.

(63) Wong E. L.; Belles, F. E. *Chem. Abstr.* **1972**, *76*, 183261; *NASA Tech. Note* **1975**, D-6495.

(64) Singleton, D.; Cvetanovic, R. *Int. J. Chem. Kinet.* **1975**, *13*, 301.

(65) Brown, R. D. H.; Smith, I. W. M. *Int. J. Chem. Kinet.* **1975**, *7*, 301.

(66) Park, C. *J. Phys. Chem.* **1977**, *81*, 499.

(67) Ravishankara, A. R.; Smith, G.; Watson, R. T.; Davis, D. D. *J. Phys. Chem.* **1977**, *81*, 2220.

(68) Hack, W.; Mex, G.; Wagner, H. G. *Ber. Bunsen-Ges. Phys. Chem.* **1977**, *81*, 677.

(69) Butler, J. E.; Hudgens, J. W.; Lin, M. C.; Smith, I. W. M. *Chem. Phys. Lett.* **1978**, *58*, 216.

(70) Baulch, D. L.; Duxbury, J.; Grant, S. J.; Montague, D. C. *J. Phys. Chem. Ref. Data* **1981**, *10*, Suppl 1.

(71) Baulch, D. L.; Cox. R. A. R.; Hampton, F., Jr.; Kerr, J. A.; Troe, J.; Watson, R. T. *J. Phys. Chem. Ref. Data* **1984**, *13*, 1259.

(72) Mahmud, K.; Kim, J. S.; Fontijn, A. *J. Phys. Chem.* **1990**, *94*, 2994.

(73) Arnoldi, D.; Wolfrum, J. *Chem. Phys. Lett.* **1974**, *24*, 234.

(74) Brown, R. D. H.; Glass, G. P.; Smith, I. W. M. *Chem. Phys. Lett.* **1975**, *32*, 517.

(75) Karny, Z.; Kartz, B.; Szoke, A. *Chem. Phys. Lett*. **1975**, *35*, 100.

(76) MacDonald, R. G.; Moore, C. B. *J. Chem. Phys*. **1978**, *68*, 513.

(77) Kneba, M.; Wolfrum, J. *Proceedings of the 17th International Symposium on Combustion*; Combustion Institute: Pittsburgh, PA, 1979; p 497.

(78) Fast, P. L.; Sánchez, M. L.; Truhlar, D. G. *Chem. Phys. Lett*. **1999**, *306*, 407.

(79) Fast, P. L.; Corchado, J. C.; Sánchez, M. L.; Truhlar, D. G. *J. Phys. Chem. A* **1999**, *103*, 5129−5136.

(80) Tratz, C. M.; Fast, P. L.; Truhlar, D. G. *PhysChemComm.* **1999**, *2/Article 14*, 1.

(81) Fast, P. L.; Truhlar, D. G. *J. Phys. Chem. A* **2000**, *104*, 6111.

(82) Peterson, K. A.; Ramachandran, B. Work in progress.

(83) Skokov, S.; Peterson, K. A.; Bowman, J. M. *J. Chem. Phys*. **1998**, *109*, 2662. Peterson, K. A.; Skokov, S.; Bowman, J. M. *J. Chem. Phys*. **1999**, *111*, 7446. Skokov, S.; Peterson, K. A.; Bowman, J. M. *Chem. Phys. Lett*. **1999**, *312*, 494.